Crack Propagation in Lead-Free Solder under Cyclic Loading of Mode I and II

K. Tanaka[1]

[1] Department of Mechanical Engineering, Meijo University, Shiogamaguchi, Nagoya 468-8502, Japan, ktanaka@ccmfs.meijo-u.ac.jp

ABSTRACT. *Crack propagation tests of lead-free solder were conducted using center-cracked plates for cyclic tension-compression and thin-walled tubular specimens for cyclic torsion. Both specimens have an initial notch as a crack starter. In fatigue loading with fast loading rates, the path of crack propagation under tension-compression was macroscopically straight, perpendicular to the maximum principal stress direction. In tubular specimens under cyclic torsion, at the high strain range, the crack propagate in shear mode II along the maximum shear direction. At low strain range, four cracks are formed from the initial silt and propagate showing macroscopically tensile mode. The introduction of creep components by tension hold propromoted shear-mode crack propagation under tension compression. For fatigue loading, the crack propagation rate was expressed as a power function of the fatigue J-integral and the relation was not much different between tension-compression and cyclic torsion. The tension hold, or the creep component, during tension-compression loading greatly accelerates the crack propagation rate. Both cycle-dependent fatigue propagation and time-dependent creep-fatigue propagation of cracks took place by joining microcracks formed along the maximum shear planes ahead of the crack tip.*

INTRODUCTION

The durability and reliability of lead-free solder joints heavily depend on the fatigue and creep-fatigue properties of solder alloys. Solder joints are subjected to thermal strain cycling induced by the mismatch of thermal expansion coefficient between components in service. Since most of the life of solder joints is spent in crack propagation, the crack propagation behavior is more important for life prediction than the crack initiation behavior. The *J* integral has been successfully used as a fracture mechanics parameter to fatigue crack propagation in solder under mode I loading [1~4]. Not many works have been conducted on fatigue crack propagation under mode II shear loading [5]. The wave shape of loading is another important factor influencing the crack porpagtaion behavior. When the loading is made at a slow rate or is held constant in tension, crack acceleration is expected due to creep contribution even tetsed at room tempearture, beause of a low melting tempearture of solder alloys. The *J* integral has also been

applied to creep-fatigue crack propagation in metallic materials at high tempeartures [6], but has not been applied to solder alloys.

In the present paper, crack propagation tests of lead-free solder were conducted using center-cracked plates (CCP) for cyclic tension compression and thin-walled tubular specimens for cyclic torsion. The *J* integral was applied to crack propagation under cyclic tension-compression and torsion. The effects of the loading wave shape and tension hold time on crack propagation were examined under tension-compression loading. The path of crack propagation was discussed as a function of the loading conditions.

EXPERIMENETAL PROCEDURE

Experimental Materials and Specimens

The experimental material was lead-free solder with the chemical compositions: Sn-3.0Ag-0.5Cu. Two types of specimens were machined from cast bars. CCP specimens used for cyclic tension-compression tests had a width of 16 mm and a thickness of 6 mm, and a through-thickness slit of 5 mm was introduced at the specimen center. Cyclic torsion tests were conducted using hollow cylinders with the outer diameter of 16 mm, the inner diameter of 13 mm, and the gage section of 30 mm in length. An initial slit was introduced perpendicular to the longitudinal axis at the middle of the gauge section of the specimen to have the length about 2 mm. All the specimens were polished with 1 μm alumina powder and annealed at 429 K for 24 h to stabilize the microstructure before fatigue tests. The microstructure consists of initially crystallized β-Sn and eutectic phase of β-Sn and Ag_3Sn.

Fatigue Testing

Fatigue tests were conducted in computer-controlled electro-servo hydraulic tension-compression and tension-torsion fatigue testing machines.

The loading waves applied to CCP specimens were vairied from fatigue dominant to creep dominant waves as shown in Fig. 1. The strain was calculated from the displacement of the gauge distance of 20 mm apart in the gauge section of CCP speciemns. Fatigue-dominant triangular waves shown in Fig. 1(a), named pp waves, were applied under displacement- or load-controlled conditions and the strain rate was set to be equal to or faster than $\dot{\varepsilon}$ =0.5%/s. In displacenent-controlled tests, the displacement ratio of the maximum to minimum displacement was -1. The strain ranges tested were $\Delta\varepsilon$ =0.05, 0.2, 0.4, 0.6, and 0.85 %. In load-controlled tests, the maximum (tensile) load was kept constant and the minimum (compressive) load was adjusted to prevent tensile ratcheting deformation.

The effect of the creep component on crack propagation was tested by four types of loading waves as shown in Fig. 1, where (b) shows slow-fast loading (cp wave), (c) is slow-slow loading (cc wave), (d) is the load wave with tension hold (cp-th wave), and (e) is the load wave with tension and compression holds (cc-th wave). The former two were displacement-controlled and the latter two load-controlled. The loading rate was

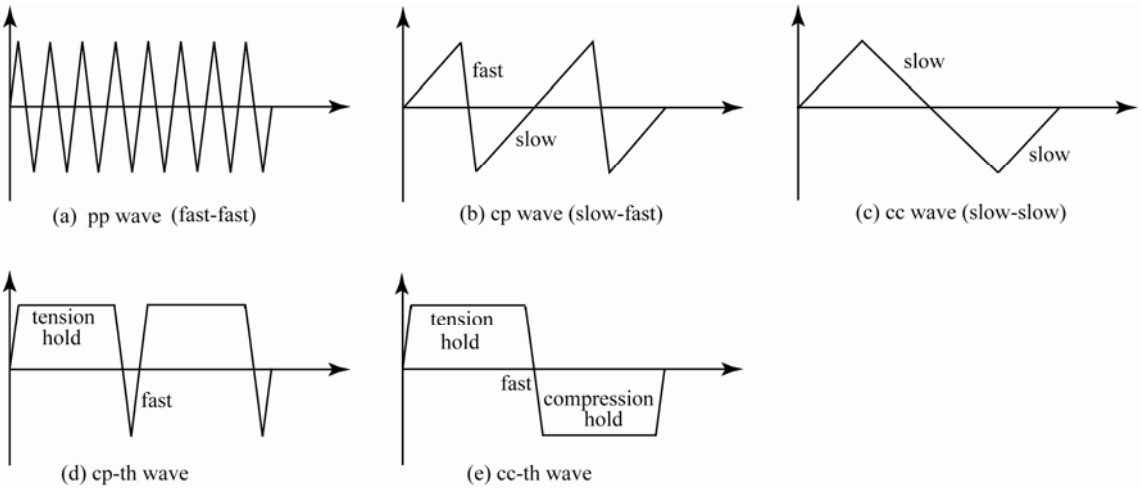

Figure 1. Loading wave forms.

8.9kN/s which gave the strain rate faster than $\dot{\varepsilon}$ =0.5%/s.

In cyclic torsion tests, the twist angle of the gage length of 25 mm was controlled. The strain wave is triangular with zero mean strain. The shear strain rate was $\dot{\gamma}$ =0.866 %/s which is the same equivalent strain rate as $\dot{\varepsilon}$ =0.5%/s used for fatigue-dominant loading in tension compression. The strain ranges tested were $\Delta\gamma$ =0.087, 0.173, 0.346, 0.698, and 1.039 %.

The crack length was measured with an optical microscope.

J-Integral Evaluation

For fatigue cracks under pp wave loading, the *J*-integral value was evaluated using a simple estimation procedure from the relation of load to the displacement at load points or to the crack-center opening displacement [7,8]. For CCP specimens under tension compression, the fatigue *J* integral, ΔJ_f, was evaluated by

$$\Delta J_f = \frac{(\Delta K)^2}{E} + \frac{S}{B(W-a)} \tag{1}$$

where ΔK is the range of stress intensity factor correspoding to the load range ΔP^*, E is Young's modulus, a is the half crack length, B is the thickness, W is the half width of the specimen, and S is the area in the load-displacement relation shown in Fig. 2(a) [7]. For torsional specimens, the ΔJ_f value is evaluated from the relation between torque and angle of twist by

$$\Delta J_f = \frac{S^*}{2B(\pi R-a)} \tag{2}$$

where R is the radius of the bar and S^* is area shown in Fig. 2(b) [9]. For the cases of cp-th or cc-th waves applied to CCP specimens, the fatigue component

of *J* integral, ΔJ_f, occurs during the loading part and the creep component of *J* integral, ΔJ_c, during tension hold. The later means the integral of creep *J* integral during one cycle. They are evaluated from the relation between load and displacement as follows:

$$\Delta J_f = \frac{(\Delta K)^2}{E} + \frac{S_p}{B(W-a)} \tag{3}$$

$$\Delta J_c = \frac{m-1}{m+1} \cdot \frac{S_c}{2B(W-a)} \tag{4}$$

where *Sp* and *Sc* are shown in Fig. 3 and *m* is the exponent of Norton's law [6].

Microscopic Observation

The microscopic observation near cracks was conducted using a scanning electron microscope (SEM, JEOL JSM-6500F, JSM-7000F) on the surface of the specimens after fatigue tests.

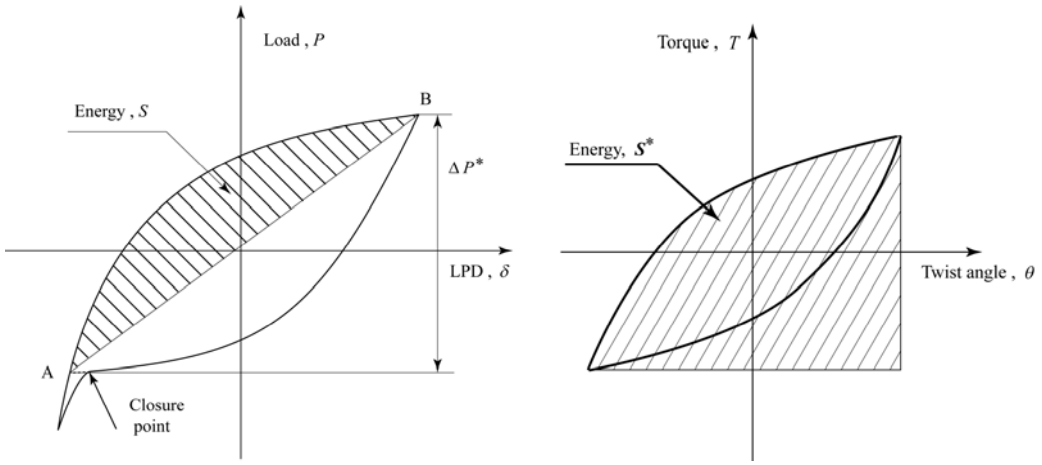

(a) Tension compression (b) Cyclic torsion

Figure 2. Evaluation of fatigue *J* integral for tension-compression and cyclictorsion.

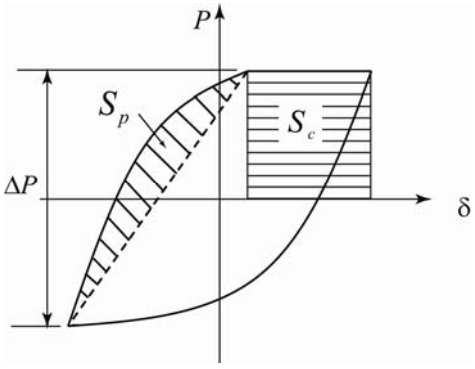

Figure 3. Evaluation of fatigue and creep *J* integrals for creep-fatigue loading.

EXPERIMENTAL RESULTS AND DISCUSSION

Crack Propagation Path

Fatigue cracks under cyclic tension compression

The crack propagated two slightly different ways depending on the applied strain range for displacement-controlled tests. Examples of fatigue cracks emanating from the initial notch are shown in Fig. 4, where (a) is at $\Delta\varepsilon = 0.2\%$ and (b) at $\Delta\varepsilon = 0.8\%$. The crack propagated nearly straight under pp waves of cyclic tension-compression below $\Delta\varepsilon$ =0.6 in CCP specimen. At a high strain range of $\Delta\varepsilon$ =0.8%, two cracks are formed from the initaial notch and only one crack extends longer. A macroscopic direction of crack path is nearly perpendicular to the loading axis, altough there is some deviation near the notch. For the case of load-controled tests, the crack path was also nearly perpendicular to the loading axis except for the case of high loads where two cracks were formed as in the case of high strain ranges.

Fatigue cracks under cyclic torsion

In tubular specimens under torsional loading, the crack propagated two distinctly different ways depending on the applied strain range. Examples of fatigue cracks emanating from the initial notch are shown in Fig. 5, where (a) is at $\Delta\gamma = 0.173\%$ and (b) at $\Delta\gamma = 0.346\%$. At the low strain range, four cracks are formed from the initial silt. The angle between two cracks is about 80 to 90 degree. The crack propagation direction is nearly perpendicular to the maximum principal stress or strain direction. On the other hand, at the high strain range, the crack propagates along the initial notch direction; the crack propagates in shear mode along the maximum shear direction. The transion takes place between the strain ranges of 0.346 and 0.173 %. This transition of the crack propagation mode in solder is first found in the present study, although similar transition has been reported for metallic materials [10].

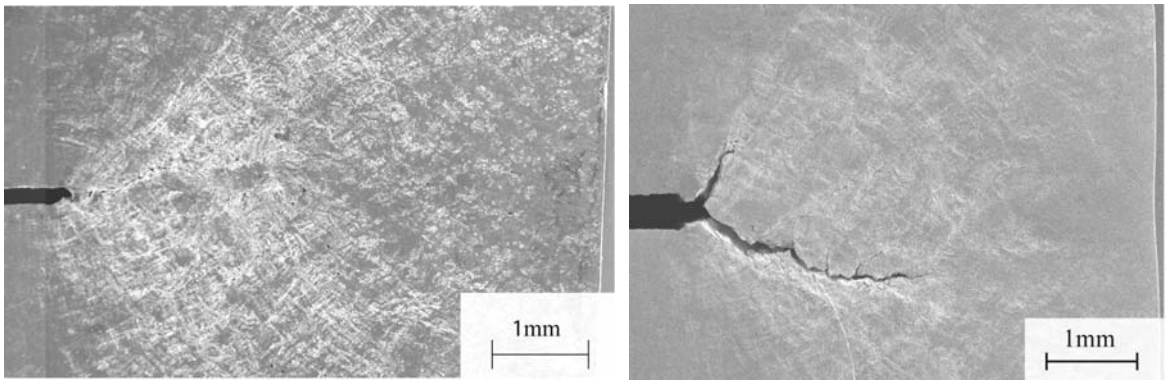

(a) pp-wave $\Delta\varepsilon = 0.2\,\%$ (b) pp-wave $\Delta\varepsilon = 0.8\,\%$

Figure 4. Crack propagation under displacement-controlled tension-compression.

(a) pp-wave $\Delta\gamma = 0.173\,\%$.

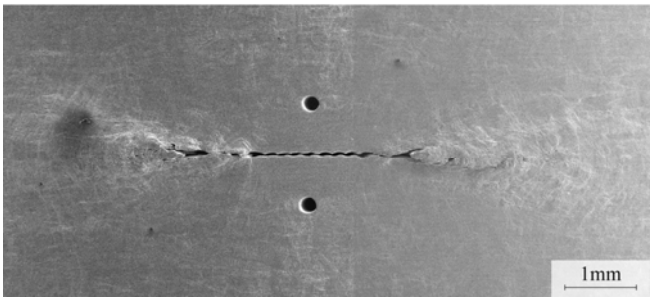

(b) pp-wave $\Delta\gamma = 0.693,\ 1.039\,\%$.

Figure 5. Crack propagation under displacemen-controlled cyclic torsion.

Creep-fatiguee cracks under tension compression with hold time

The path of crack propagation is very much infuenced by the introduction of creep components. The crack propagates along the maximum shear direction under cc wave. The path under cp wave also tends to follow the maximum shear direction. The creep component pronouces the shear-mode crack propagation even at the same applied strain range. For the case of load controlled tests with the hold time, the shear mode crack propagation is more pronouced under cc-th wave than under cp-th wave as shown in Fig. 6. The angle between two cracks emanating from the notch is 94 degree for cp-th wave and 102 degree for cc-th wave.

.

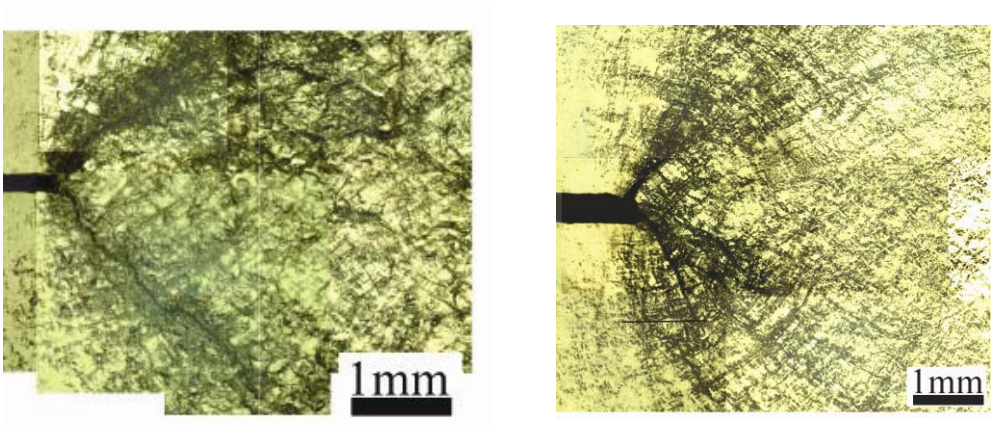

(a) cp-th wave (b) cc-th wave

Figure 6. Crack propagation under load-controlled tension-compression with cp-th and cc-th waves.

Crack Propagation Rate

Fatigue cracks

The projection of the maximum crack length on the plane perpendicular to the longitudinal direction of the specimen was measured for both tension-compression and torsion loadings. The half of the sum of the actual crack and the notch length was taken as the crack length *a*. The *J* integral was determined from the relation between the load and the displacement recorded during fatigue using simple estimation methods described above.

For the displacement-controlled tests including pp, cp, and cc waves, the crack propagation rate and the *J* integral range were nearly constant while the crack length extended from 2.7 to 5.0 mm. Since the crack propagation rate and the fatigue *J* integral were nearly constant for the displacement-controlled tests, the measured values were averaged for each case. On the other hand, in load-controlled tests including pp, cp-th, and cc-th waves, both the crack propagation rate and the *J* integral increase with the crack length.

Figure 7 shows the relation between the crack propagation rate and the fatigue *J* integral for pp waves under tension compression. For both cases of dispalcement- and displacement-controlled tests, the crack propagation rate d*a*/d*N* (m/cycle) is expressed as the following power function of the fatigue *J* integral (N/m) :

$$da/dN = 7.96\times10^{-12}\left(\Delta J_f\right)^{1.34} \qquad (5)$$

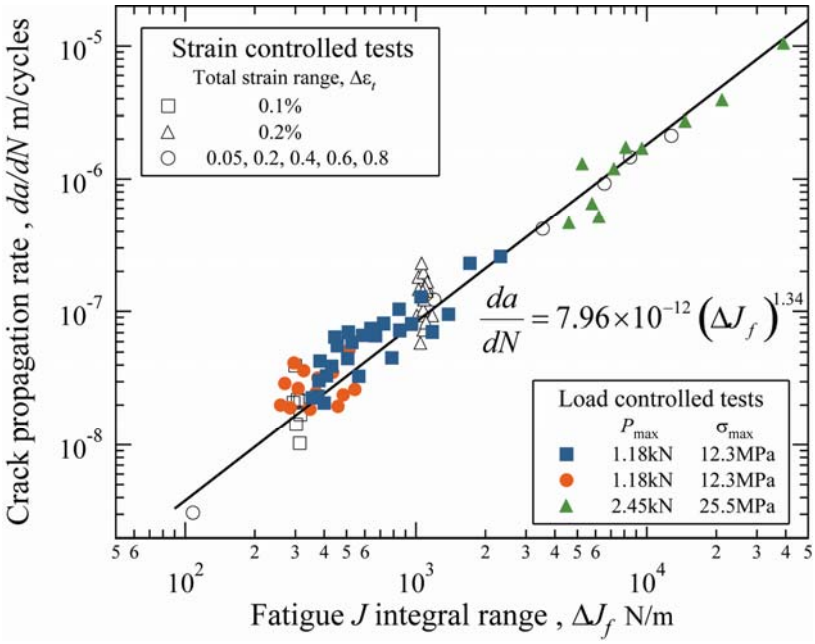

Figure 7. Relation between crack porpagation rate and fatigue *J* integaral for pp waves under dsialacement- and load-controlled tension-compression.

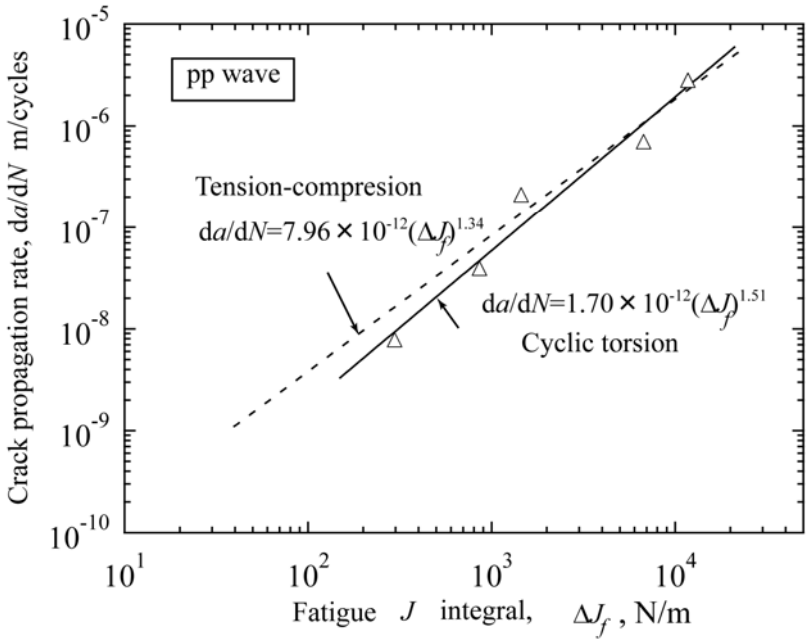

Figure 8. Relation between crack porpagation rate and fatigue *J* integaral for pp waves under dsialacement-controlled cyclic torsion.

The relation obtained for torsion loading is shown in Fig. 8, where Eq. (5) is shown with the solid line. At large ΔJ_f values, the rate is about the same between tension compression and torsion, while it is slightly larger for tension-compression at low ΔJ_f values. The following power relation is obtained for cyclic torsion by linear regression:

$$da/dN = 1.70 \times 10^{-12} \left(\Delta J_f \right)^{1.51} \tag{6}$$

There is no large difference in the relation between tensile-mode and shear-mode crack propagations as far as the crack propagates by fatigue.

Creep-fatigue cracks

Figure 9 shows the hysteresis loops between displacement and load obtained at the crack length of 3.40 mm for various waves of load-controlled conditions. The tensile hold in cp-th and cc-th waves introduces the creep component of the *J* integral, while pp wave gives only the fatigue *J* intergral. The values of ΔJ_f and ΔJ_c were determined from the relation between displacement and load by using the simple estimate method described in Fig. 3.

Creep-fatigue crack propagation rate per cycle d*a*/d*N* is plotted against the fatigue *J* integral ΔJ_f in Fig. 10, where the solid line indicates the relation of Eq. (5) for fatigue crack propagation under tension compression with pp waves. When compared at the same *J* integral, the creep component of loading accelerates the crack propagation rate. In the displacement-controlled tests, the amount of crack acceleration is smaller for cc

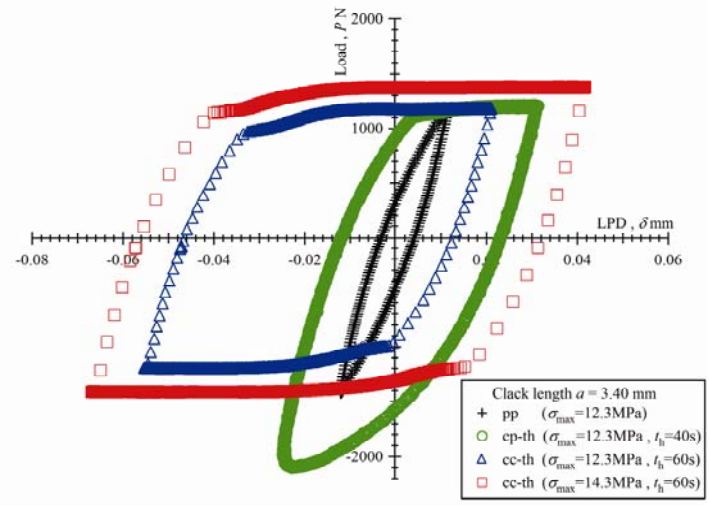

Figure 9. Hysteresis loops of load vs displacement for tension-compression with pp, cp-th, and cc-th waves.

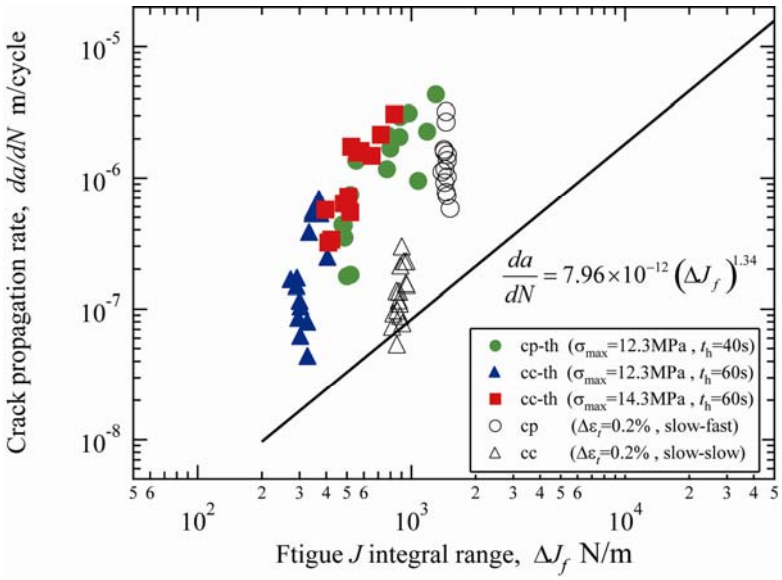

Figure 10. Relation between crack porpagation rate and fatigue *J* integaral for tension-cmpression with cp. cc, cp-th, and cc-th waves.

wave than for pc wave. For the case of load-controlled tests, tension hold greatly increases the crack propagation rate; the acceleration is the largest for cp-th wave.

The total *J* integral was caluculated as the sum of fatigue and creep components:

$$\Delta J_t = \Delta J_f + \Delta J_c \qquad (7)$$

In Fig. 11, the crack propagation rate is plotted gainst the total *J* integral for load-controlled tests. The crack propagation rate under cp-th wave is twenty times faster than that under pp-wave when compared at the same ΔJ_t value.

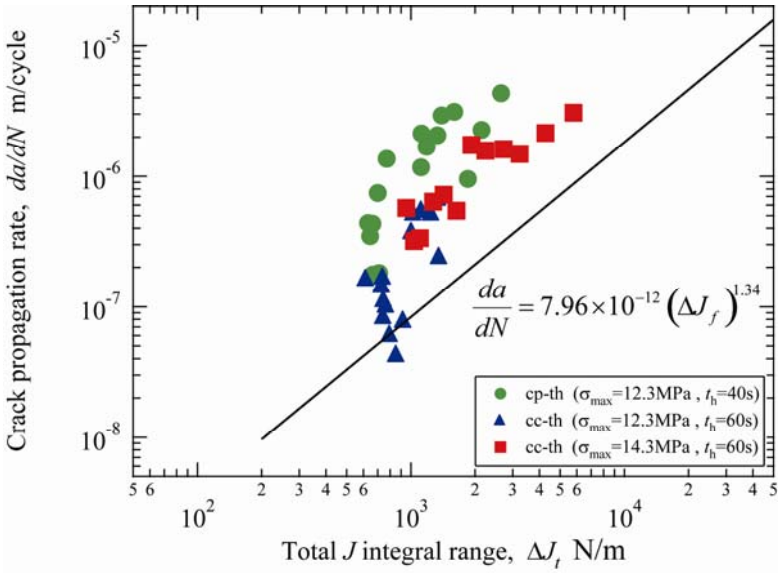

Figure 11. Relation between crack porpagation rate and total *J* integaral for tension-cmpression with cp-th, and cc-th waves.

Microscopic Observation

Many microcracks were observed ahead of the main crack tip for both tension-compression and torsional loadings. Figure 12 shows SEM micrographs near the tip of the main crack under displacement-controlled tension-compression with pp wave of $\Delta\varepsilon = 0.2\%$. Many microbranchings and microcracks can be seen around main crack, microcracks are formed along grain boundaries and along slip bands.

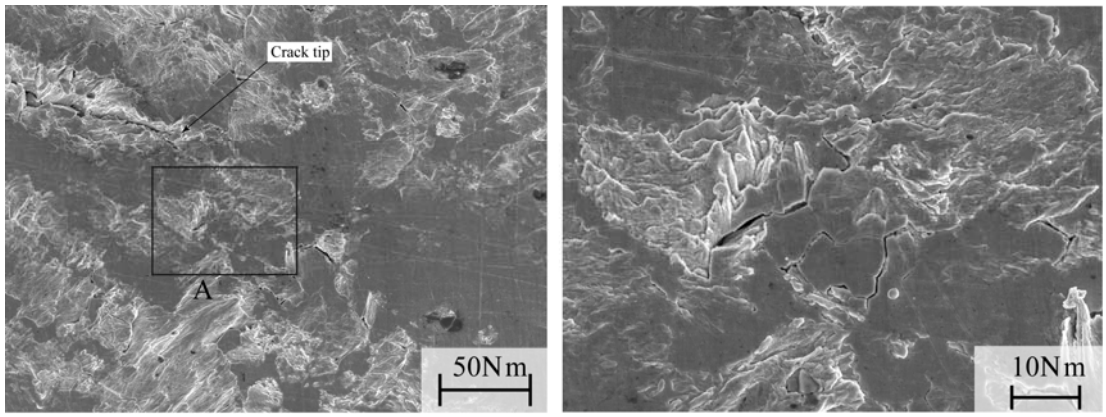

(a) Crack-tip region (b) Enlargement of part A

Figure 12. SEM micrographs near the tip of crack under displacement-controlled tension compression with pp-wave of $\Delta\varepsilon = 0.2\,\%$.

Figure 13 shows SEM micrographs near the crack tip for torsional loading with pp wave of $\Delta\gamma = 0.346\%$. Microcracks extend either horizontally or vertically along the maximum shear direction in the heavily deformed zone ahead of the crack tip. Some fragmentation of grains is seen near the crack tip. At low strain ranges, the crack propagates joining shear microcracks and leaving zig-zag shape, although the crack propagated macroscopically tensile mode.

The introduction of creep components enhanced the shear-mode crack propagation as shown in Fig.14, where is the case of cc-th wave under tension compression. The fragmentation of grains is abundant near the crack as seen in Fig. 14(b), and also microcracks and microbranchings are seen around the main crack.

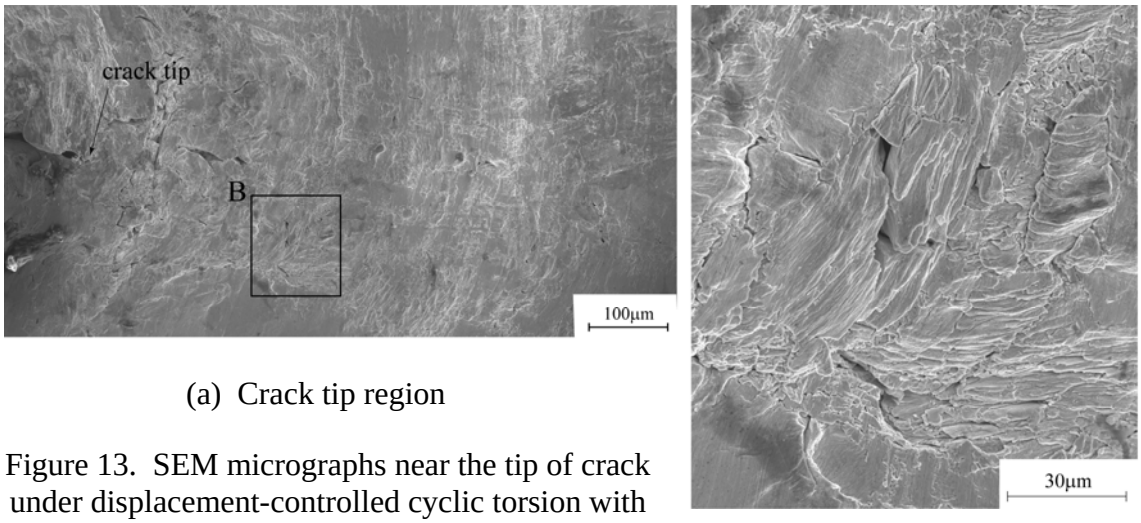

(a) Crack tip region

(b) Enlargement of part B

Figure 13. SEM micrographs near the tip of crack under displacement-controlled cyclic torsion with pp-wave of $\Delta\gamma = 0.364\%$.

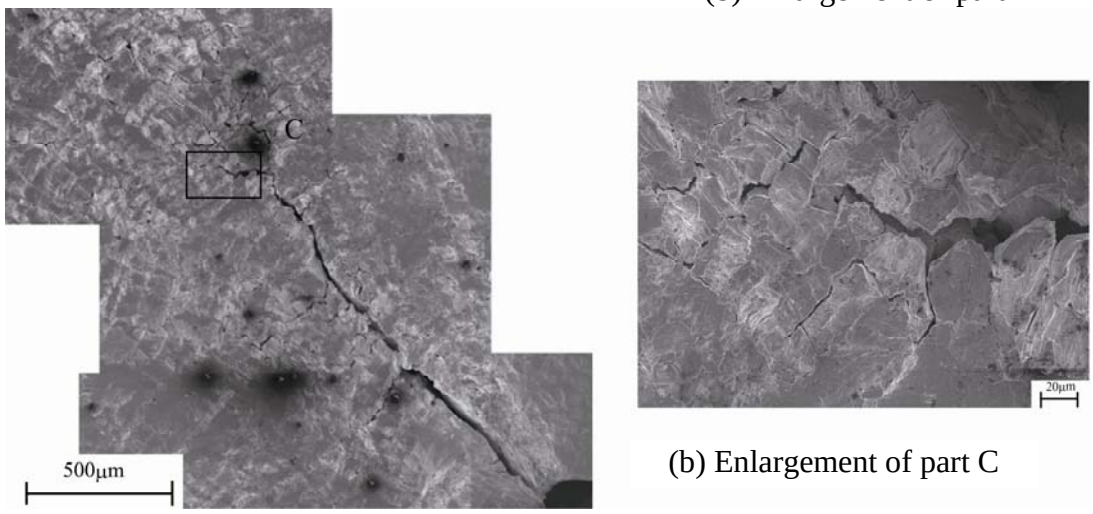

(a) Crack tip region

(b) Enlargement of part C

Figure 14. SEM micrographs near the tip of crack under load-controlled tension-compression with cc-th wave.

Figure 15 illustrates microcracks formed near the notch tip along the maximum shear directions which are indicated by grids making ± 45 deg with respect to the loading axis. Under high stresses or large creep contributions, the crack propagate by connection microcracks with angles of 45 deg, which results in macroscopically shear mode propagation. On the other hand, under low stress, the length of microcracks is small and the crack propagates only by a small amount in the shear direction and then makes a turn to the opposite direction, resulting in macroscopically tensile-mode propagation.

A similar model for crack propagation-mode transition can be applied to torsion fatigue as shown in Fig. 16. At high strain ranges, many microcracks are formed horizontally as well as vertically ahead of the main crack and the main crack propagates coplanar by joining these horizontal microcracks. At low strain ranges, the amount of microcracks is limited and the crack deviates by connecting vertical microcrarcks, showing macroscopically tensile-mode propagation.

The quantutative analysis of the condition of the mode transition of crack propagation is underway and the criterion will be expressed in terms of the inelastic components of local near-tip strains determined by the finite element method.

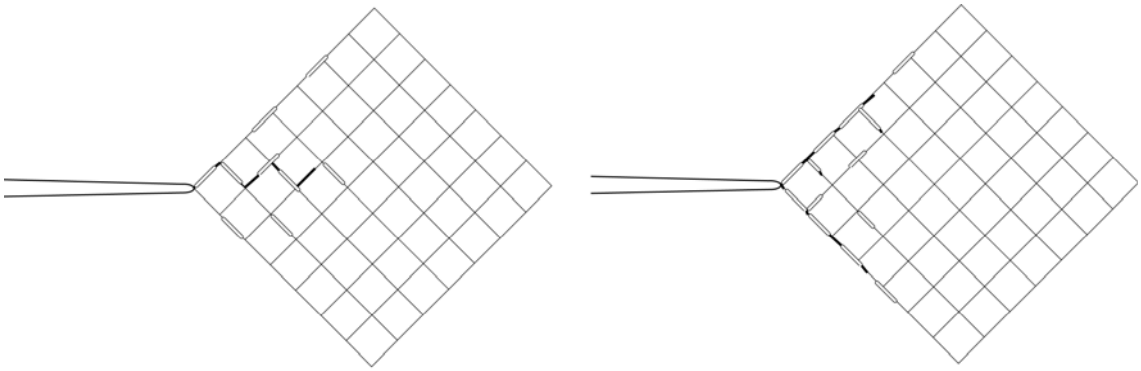

(a) Tensile-mode crack propagation at low stress

(b) Shear mode crack propagation at high stress or creep-dominant condition

Figure 15. Crack propagation mode under cyclic tension-compression.

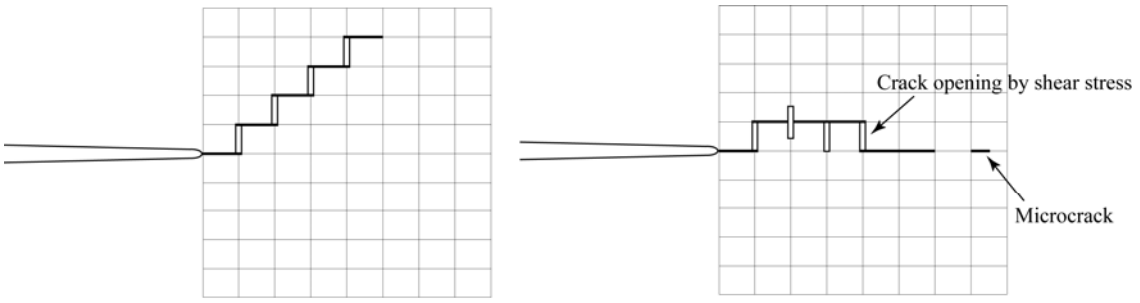

(a) Tensile-mode crack propagation under cyclic torsion at low strain range

(b) Shaer-mode crack propagation under cyclic torsion at high strain range

Figure 16. Crack propagation mode under cyclic torsion.

CONCLUSIONS

(1) The path of crack propagation under pp wave in center-cracked specimens under tension-compression was macroscopically straight, and perpendicular to the maximum principal stress direction. Contributions of creep components deviated the crack propagation mode to shear mode
(2) In tubular specimens under pp wave of torsional loading, at high strain ranges, the crack propagates in shear mode along the maximum shear direction. At low strain ranges, four cracks are formed from the initial silt and propagate showing macroscopically tensile-mode.
(3) For fatigue loading by pp wave, the relation between the rate, d*a*/d*N*(m/cycle), and the fatigue *J* integral, ΔJ_f (N/m), is expressed as

$$da/dN = 7.96\times10^{-12}\left(\Delta J_f\right)^{1.34}$$

for cyclic tension-compression and

$$da/dN = 1.70\times10^{-12}\left(\Delta J_f\right)^{1.51}$$

for cyclic torsion. The difference is small.
(4) The crack propagation is accelerated by the introduction of creep components. The tension hold acecelerates the propagation rate of creep-fatigue cracks by twenty times faster than that under pp-wave when compared at the same total value of the *J* integral.
(5) Both cycle-dependent fatigue propagation and time-dependent creep-fatigue propagation of cracks took place by joining microcracks formed along the maximum shear planes ahead of the crack tip.

REFERENCES

[1] H. Takahashi, M. Mukai and T. Kawakami (2000) *Trans. Japan Society Mechanical Engineers*, Vol. 66, pp. 1343-1349.

[2] K. Terasaki, M. Kitano and H. Miura (2000) *Trans. Japan Society Mechanical Engineers*, Vol. 66, pp. 1506-1511.

[3] H. Nose, M. Sakane, M. Yamashita and K. Shiokawa (2002) *Trans. Japan Society Mechanical Engineers*, Vol. 68, pp. 88-95.

[4] J. Zhao, Y. Mutoh, Y. Miyashita and L. Wang (2003) *Eng. Fract. Mech.*, Vol. 70 pp. 2187-2197.

[5] H. Nose, M. Sakane, M. Yamashita and K. Shiokawa (2003) *Trans. Japan Society Mechanical Engineers*, Vol. 69, pp. 1222-1229.

[6] S. Taira, R. Ohtani, T. Kitamura and K. Yamada (1979) *Journal Materi. Sci. Japan*, Vol. 28, pp. 414-420.

[7] J. R. Rice, P.C. Paris and J.G. Merkle (1973) *ASTM STP* 536, pp. 231-245.

[8] N. E. Dowling (1976) *ASTM STP* 601, pp. 19-32.

[9] K. Tanaka, Y. Iwata and Y. Akiniwa (2008-9) *Proceedings of the 17th European Conference on Fracture*, p. 150, CD-ROM.

[10] C. Pinna and V. Doquet (1999) *Fatigue Fract. Engng Mater. Struct.*, Vol. 22, pp. 173-183.